ACS OMEGA

http://pubs.acs.org/journal/acsodf

Article

Radioiodination of Modified Porous Silica Nanoparticles as a Potential Candidate of Iodine-131 Drugs Vehicle

Maria Christina Prihatiningsih, Teguh Ariyanto, Edy Giri Rachman Putra, Veronika Yulianti Susilo, Isa Mahendra, and Imam Prasetyo*

Cite This: *ACS Omega* 2022, 7, 13494−13506

Read Online

ACCESS | Metrics & More | Article Recommendations | Supporting Information

ABSTRACT: There are challenges related to cancer treatment, namely, targeting and biocompatibility associated with a drug vehicle. This research aims to prepare a theranostic cancer vehicle based on porous silica nanoparticles (PSN) with controllable nanoparticle size, supporting targeting properties, and biocompatible. The synthesis method combined the Stöber process and liquid crystal templating using a dispersant and pore expander. Triethanolamine (TEA) and Pluronic F-127 were combined as a steric stabilizer and dispersing agent, while *n*-hexane was used as a pore expander. The amine functionalization was carried out using the 3-aminopropyl-triethoxysilane solution. Furthermore, radiolabeling of PSN using Iodine-131 and iodogen as oxidizing agents was carried out. The results showed that the best achievable PSN size was 100−150 nm with a polydispersity index of 0.24 using TEA-Pluronic F-127. The functionalization results did not significantly affect the radioiodination result. Radiochemical purity (RCP) values up to 95% were obtained in the radioiodination, while the labeled compounds were relatively stable with 12 mCi radioactivity, indicating the absence of radiolysis. The synthesized PSN was not toxic to normal cell samples up to a concentration of 150 μg/mL for PSN and 170 μg/mL for PSN-NH_2. The cellular uptake testing results of the PSN-^{131}I in cancer cell samples showed promising uptake ability.

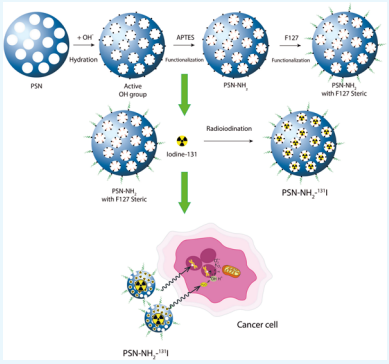

INTRODUCTION

Conventional cancer diagnosis and therapy still require prolonged and high-cost treatment due to the treatment stages, such as an initial round of treatment followed by maintenance therapy. Maintenance treatment may include chemotherapy, hormonal therapy, or targeted therapy. Therefore, a combination of diagnostic and therapeutic methods is introduced in one platform called theranostic.[1−4] With the theranostic application, many scientists hope that all matters related to time, effort, and costs can be reduced, and detection and treatment of diseases in real-time are possible.[5] On the other hand, there are also problems related to cancer treatment, namely, targeting issues, drug loading capacity, and biocompatibility.[1,6] These problems are caused by the lack of an appropriate theranostic vehicle. Radionuclides such as ^{131}I as γ emitters at 365 keV and β emitters at 606 keV can be used as theranostics agents,[7−11] by ionizing cancer cells. For thyroid malignancies, when Na^{131}I is administered, this radionuclide has good tolerability, ease of application, safety and efficacy of therapy, and highly accurate and targeted treatment with limited side effects.[12−15] In addition, radionuclide ^{131}I can be applied to diagnose and treat neuroblastoma and endocrine gland cancer in the form of ^{131}I-metaiodobenzylguanidine (^{131}I-MIBG).[16−21] ^{131}I also has potential as a drug or imaging agent in treating other cancers such as liver, prostate, breast, and other cancers,[7,18,22−24] when ^{131}I is suitably tagged on the carrier or its vehicle. Among the drug vehicles developed so far, nanovehicles such as porous silica nanoparticles (PSN) emerge as promising candidates because they can carry drug molecules for therapeutic and diagnosis[25] in a controlled manner. PSN has advantageous properties such as large pore volume, tuned pore diameter, controlled particle size, high specific surface area,[26−29] and relative ease of production. In addition, in certain forms, for example, when PSN is modified, this material is relatively stable, safe, and biocompatible for biomedical applications.[30] The Food and Drug Administration (FDA) classifies silica "Generally Recognized as Safe" (GRAS) as food additives.[31]

The PSN should have compatible functional groups e.g., amines on the surface of the PSN. Therefore, a surface decoration or functionalization of PSN is needed for biocompatibility. Replacing surface silanol groups with biocompatible molecules such as polymeric or organosilane surface modification ligands is very important to increase the biocompatibility of PSNs.[32] In addition, the active group can

Received: November 17, 2021
Accepted: April 7, 2022
Published: April 18, 2022

also change the PSN charge as needed and can be used as a drug binder so that it is relatively stable when it enters the biological system. Modification with amine functional groups on PSN with 3-aminopropyltriethoxysilane (APTES) precursor can be done by the postsynthetic grafting method. The presence of functional groups on the surface of the PSN allows interactions with the carried drug cargo.[33−35] A polymeric ligand, poly(ethylene glycol) (PEG), is the most commonly used for modification due to its good biocompatibility, hydrophilicity, and antifouling properties. However, the PEGylation process has some limitations; i.e., (i) mostly requires complex modification techniques and (ii) PSN pore can be closed during pegylation, then inhibit the drug loading process.[32]

To be used as a vehicle for radioactive drugs, PSN must be labeled with the appropriate radionuclide. There are still many limitations of nanoparticle radiolabeling,[36,37] for example, in terms of radiochemical purity (RCP) and the stability of the bond between radioactive substances and their vehicle candidate materials. Therefore, it is necessary to study the radiolabeling process for PSN compared to PSN that has been functionalized.

This research aims to prepare and label PSN with specific characteristics that can eventually be used as candidates for theranostic vehicles. The features to be achieved in this PSN preparation study are targeting, drug loading capacity, and properties that support biocompatibility. The preparation of PSN includes modification of PSN such as synthesis procedure, functionalization of the amine group, and radiolabeling with iodine-131 radioisotope. PSN was synthesized using a combination of the Stöber process and liquid crystal templating with the addition of a dispersant, a steric stabilizer, and a pore expander. The material was modified using Pluronic F127 as a substitute for PEG-silane and then functionalized using APTES. At the radiolabeling stage, there were variations in reaction time, number of oxidizing agents, radioactive labeling activity, specific surface area, and observations of the stability of compounds marked with radiolabeling results. A direct correlation between the functionalization and the PSNs radiolabeling results is evaluated and discussed.

RESULT AND DISCUSSION

Control of Nanoparticle Size in PSN Synthesis. Nanoparticles in the size range of 100−200 nm can accumulate in tumor tissue via the enhanced permeability and retention effect (EPR),[35,38] as shown in Figure 1[39] This phenomenon is called passive targeting. In the preparation of PSN, the particle size was adjusted to have passive targeting properties.

The Stöber method is reliable in controlling spherical silica nanoparticles' monodispersed properties.[40] Then, a combination of dispersant compounds and a steric stabilizer such i.e., triethanolamine (TEA) and PEG was used to design the size of the nanoparticles. Therefore, Pluronic F-127 was used as a substitute for PEG-silane.[41,42]

Figure 2 shows the effect of adding a TEA and Pluronic F127 (abbreviated as F127) combination, which can control the size and re-dispersion of PSN. Figure 2a demonstrates the experimental results of adding variation of TEA and F127 from 0 to 10 mL per gram cetyltrimethylammonium bromide (CTAB) in PSN synthesis. The best results, namely, 150 nm with a polydispersity index (PDI) value of 0.211, were achieved by the addition of TEA and F127 (7.5 mL). The pattern of the sharp dip of the graph in Figure 2a is due to the

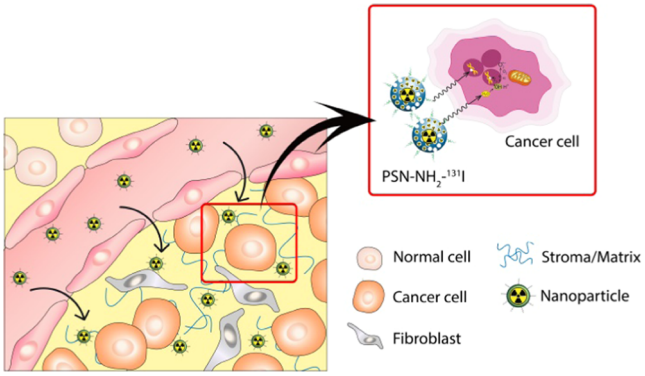

Figure 1. Illustration of PSN accumulation as a vehicle for radioactive drugs to target tumors through the EPR effect (Adapted with permission from Nakamura et al., 2016, Copyright 2016 by the American Chemical Society).[39]

fact that the addition of TEA and F-127 really affected the hydrophilic properties of the synthesized PSN. Synthesized PSN which is sometimes hydrophobic as a result of the use of organic solutions in the mixture can be changed to become more hydrophilic. According to Beltrán-Osuna and Perilla,[42] targeting properties are directly related to particle size uniformity.[43] Nanoparticles that can enter tumor tissue to get a therapeutic effect are of size less than 400 nm. Another study shows that the adequate particle size for medical applications is 150 nm.[44] With the achievement of the PSN size at 150 nm, it is hoped that PSN will qualify as a drug vehicle toward the target.

Figure 2b shows the DLS particle size distribution of PSN, which was dispersed in F-127 solution and sonicated for 30 min (z-average = 150 nm and PDI = 0.211 The z-average size varied from 149.6 to 152.7 nm with 150.4 ± 0.03 of three repetitions). Figure 2c,d shows the TEM characterization results comparing PSN synthesized with the addition of TEA + F127 vs PSN without the addition of TEA + F127. The TEM characterization results correlated with the PSA−DLS characterization data. Furthermore, the addition of TEA & F127 can produce a more desirable nanoparticle size. When observed with the TEM characterization result, the PSN images added with TEA and F-127 appeared to be the most monodispersed with a size smaller than 100 nm. When followed closely, the size of the PSN with TEM looks smaller than PSA−DLS. This size is because the measurement with PSA−DLS is a hydrodynamic measurement of the diameter of the nanoparticles. The results related to the size of the PSN align with Yismaw et al.'s research on synthesizing monodispersed PSN nanoparticles[41] that the presence of TEA and F-g127 increases the dispersity of nanoparticles.

The schematic in Figure 3 illustrates the approximate mechanism of TEA and F-127 when interacting with Si and CTAB precursors during PSN synthesis according to the literature[44−46] and the means for controlling the size of nanoparticles using F-127. Initially, the liquid crystalline mesophases or positively charged micelles of CTAB act as templates in which the negatively charged silicate ions are hydrolyzed and then condensed. In the process of hydrolysis and condensation, the initial particles of silica begin to form and then grow. In the presence of TEA, the growth of silica particles can be further inhibited. Then, with the addition of F-127, the stability of silica particles can be maintained by the F-127 self-assembly interaction.

https://doi.org/10.1021/acsomega.1c06492
ACS Omega 2022, 7, 13494−13506

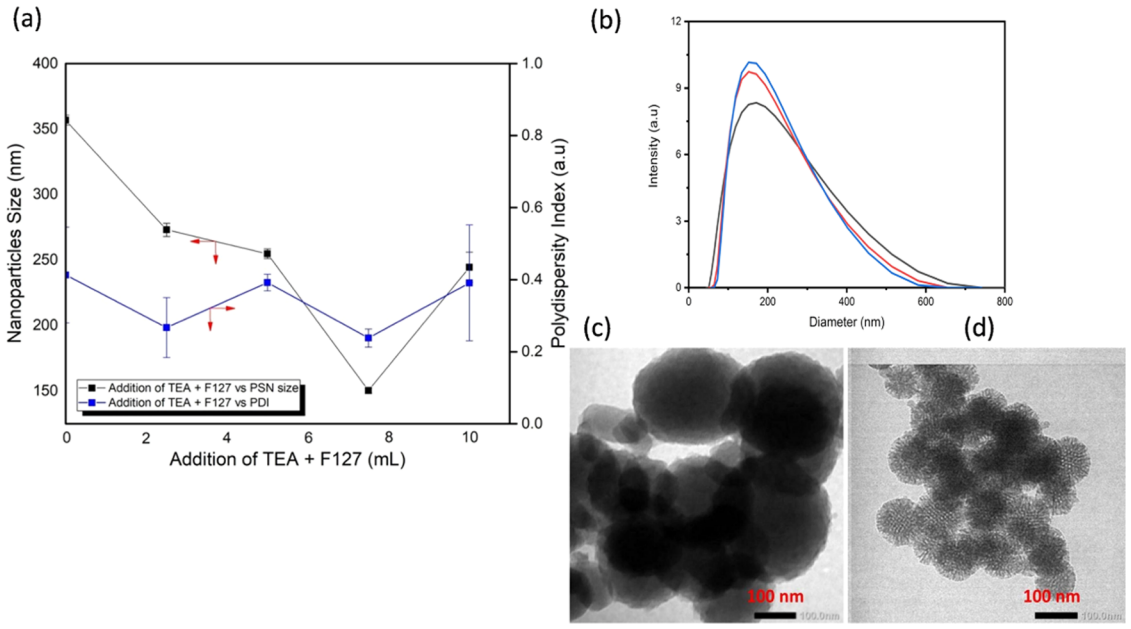

Figure 2. (a) Effect of addition of TEA and F127 on PSN size control. (b) DLS particle size distribution of PSN, which was dispersed in F-127 solution and sonicated for 30 min (z-average = 150 nm and PDI = 0.211 The z-average size varied from 149.6 to 152.7 nm with 150.4 ± 0.03 of three repetitions), (c) transmission electron microscopy (TEM) images of PSN synthesized without the addition of TEA + F127 (under 40,000 magnification) and (d) TEM images of the PSN synthesized with addition of TEA + F127 (under 40,000 magnification).

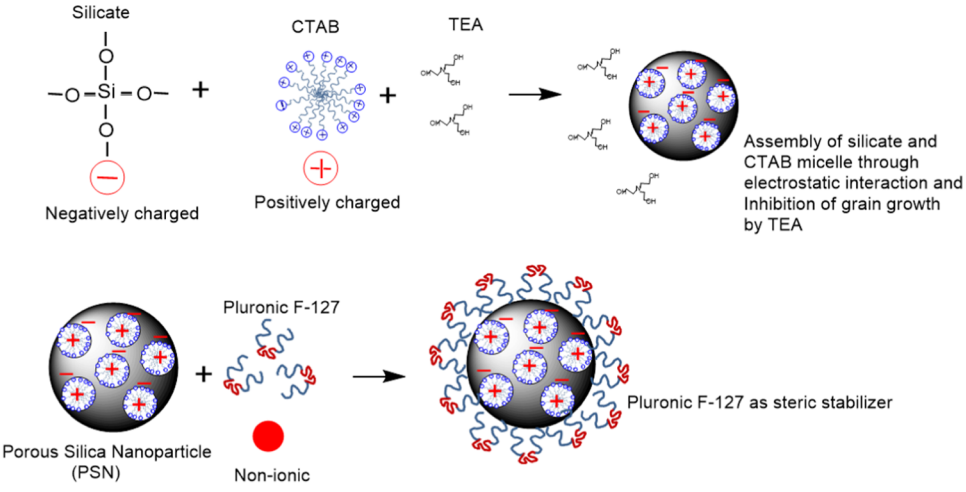

Figure 3. Mechanism of CTAB, TEA, and F-127 when interacting with PSN (Adapted with permission from Ikari et al, 2006, Copyright 2005 American Chemical Society[45]).

In controlling the size of nanoparticles, it is necessary to strive for the stability of the PSN. It uses PSA−DLS and ζ-potential, measured over a specific time as is shown in Figure 4. Figure 4a indicates that the stability of the PSN can be maintained at around 150.3 nm size for one (1) day. After a storage time of 5 days, the nanoparticle size changes to about 200 nm, and after 14 days, there was a more significant change in the size of the nanoparticles and PDI that is over 300 nm. If the experiment is carried out for up to three (3) days, the size of the nanoparticles begins to change even though it is still less than 300 nm. After 5 days and 14 days, PSN can be reconditioned by stirring and sonication so that the agglomeration is reduced and the particles are redispersed. Conditioning with sonication was carried out for approximately 30 min (see Figures S1 and S2). The ζ-potential value at the optimal synthesis condition PSN can be seen in Figure 4b that expresses the degree of electrostatic repulsion between adjacent and charged PSN particles in terms of resisting aggregation. PSN was dispersed in F-127 solution and sonicated for 30 min (solution pH = 7.5). The PSN ζ-potential value reveals that the PSN generated from this study has moderate stability, namely, at a value of 37.4 mV to incipient instability at 20.8 mV.

Controlling Surface Properties in PSN Synthesis. PSN properties such as specific surface area pore volume and pore diameter correlated with drug loading capacity. In this study, a high drug loading capacity is desired to ensure proper efficacy and low toxicity. Although the specific surface area of mesoporous silica can reach 1000 m^2/g,[46−48] this study is not obsessed with achieving these values. However, larger pore diameters are sought to provide flexibility of surface properties for functionalization. This study adopted the liquid crystal

https://doi.org/10.1021/acsomega.1c06492
ACS Omega 2022, 7, 13494−13506

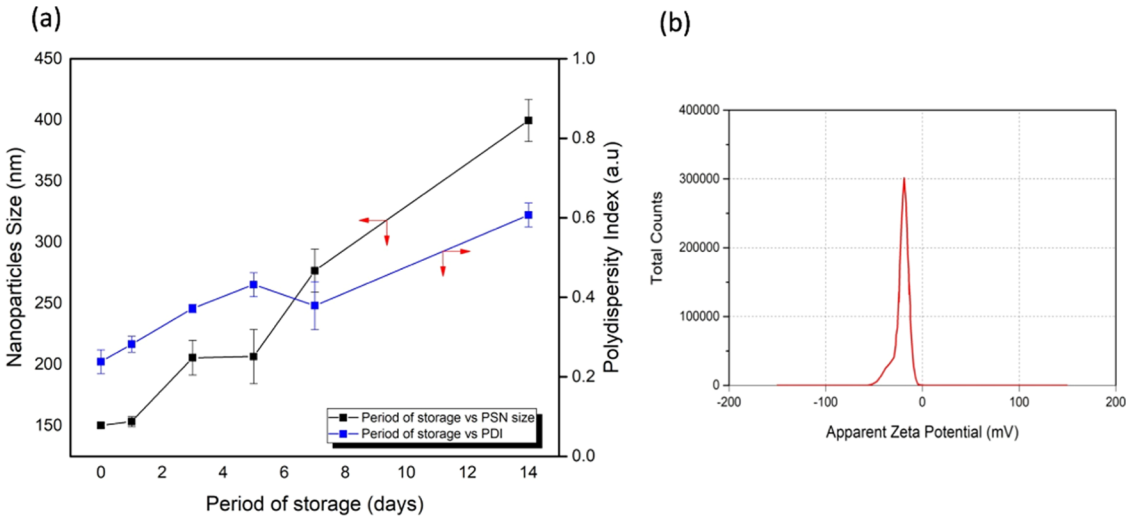

Figure 4. (a) Stability of the PSN vs period of storage. (b) ζ-Potential of PSN, which was dispersed in F-127 solution and sonicated for 30 min (solution pH = 7.5).

Table 1. Surface Properties of the PSN, PSN-NH_2, and PSN-NH_2-I Evaluated from N_2 Adsorption

description	blank PSN	PSN-NH_2 (aminated PSN)	PSN-NH_2-I (I-adsorbing PSN-NH_2)
specific surface area (m^2/g)	580.9	274.9	20.2
pore volume (cm^3/g)	0.74	0.28	0.14
mean pore diameter (nm)	5.1	4.1	2.7

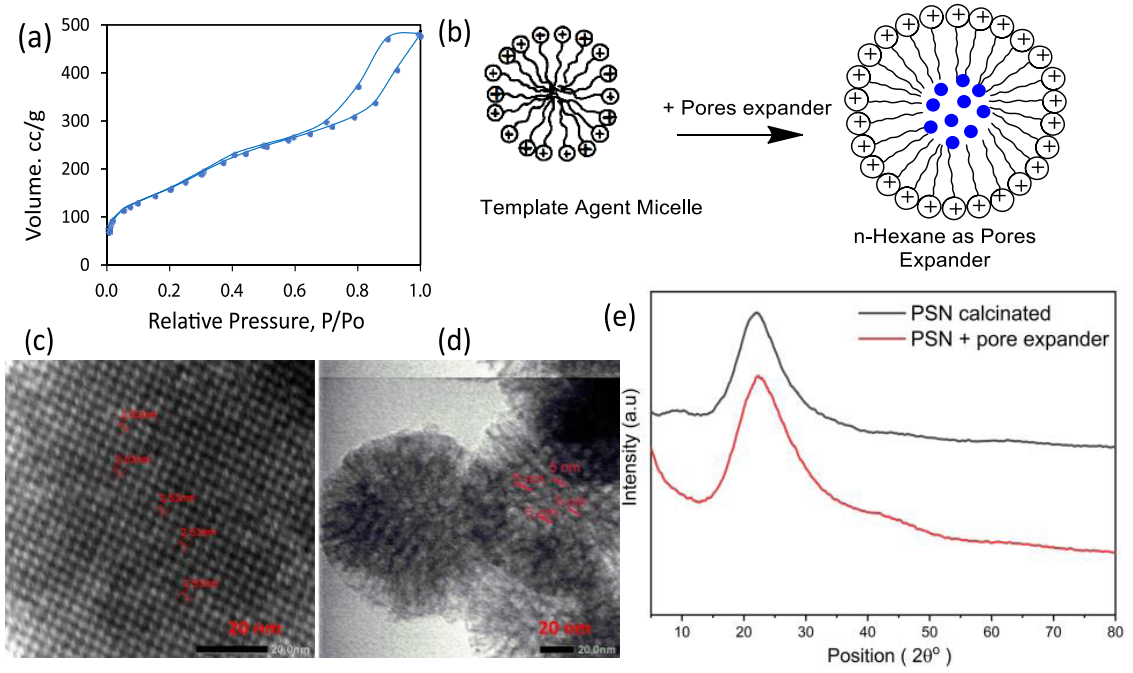

Figure 5. (a) Isotherm curve of PSN characterized by SAA Brunauer−Emmett−Teller (BET). (b) Illustration of the PSN pore-expanding using *n*-hexane. (c) TEM image of the PSN synthesized without pore expander (under 300,000 magnification). (d) TEM image of the PSN synthesized with pore expander (under 150,000 magnification). (e) PSN diffraction pattern by X-ray diffraction (XRD).

templating method to control the surface properties of PSN.[49] Surface control is carried out using a CTAB template and an organic alkane solvent such as *n*-hexane as pore expander.[50] The characterization of the surface properties using the nitrogen gas adsorption method is shown in Table 1 and Figure 5a.

Based on Table 1, it can be seen that the specific surface area that has not been functionalized PSN was 580.9 m^2/g with a pore diameter of 5.1 nm and a pore volume of 0.74 cm^3/g. The PSN isotherm curve in Figure 5a belongs to group IV in the IUPAC classification.[51] Figure 5b indicates that the interaction mechanism between *n*-hexane with CTAB is a swelling phenomenon controlled by *n*-hexane. Figure 5c shows the TEM characterization of PSN without a pore expander, while Figure 5d shows the TEM characterization of PSN with a pore expander. It shows that the diameter of the pore without using

https://doi.org/10.1021/acsomega.1c06492
ACS Omega 2022, 7, 13494−13506

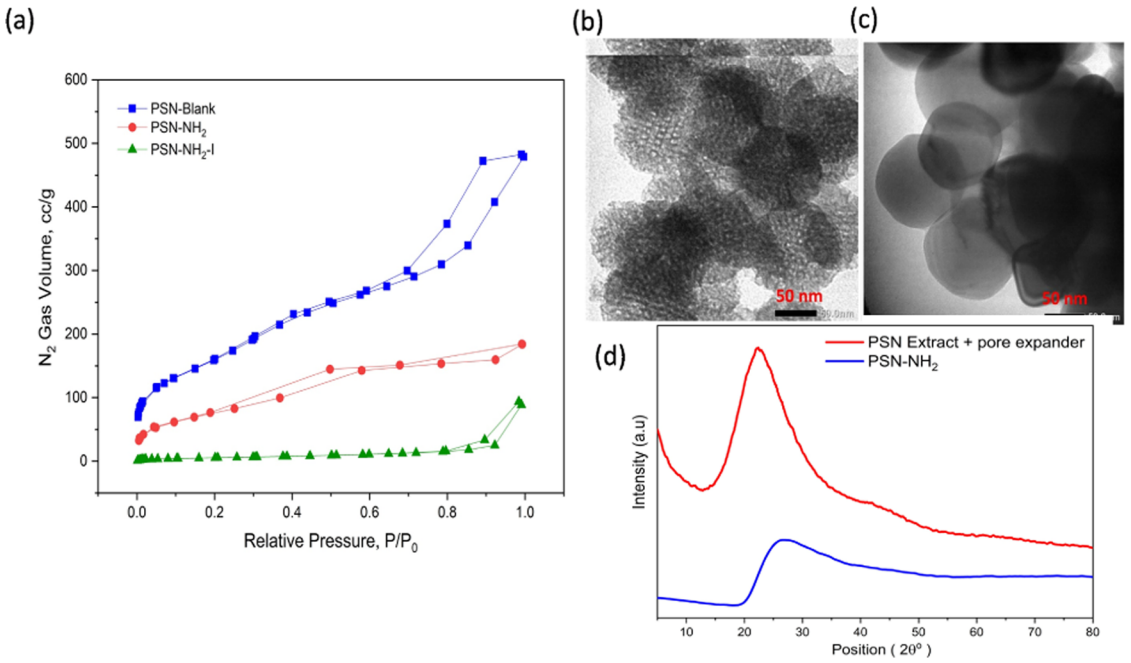

Figure 6. (a) Nitrogen adsorption−desorption isotherms of the PSN samples. (b) TEM image of the blank PSN (under 80,000 magnification). (c) TEM image of the amine-functionalized PSN (under 80,000 magnification). (d) PSN diffraction pattern by XRD compared with PSN-NH_2 diffraction pattern.

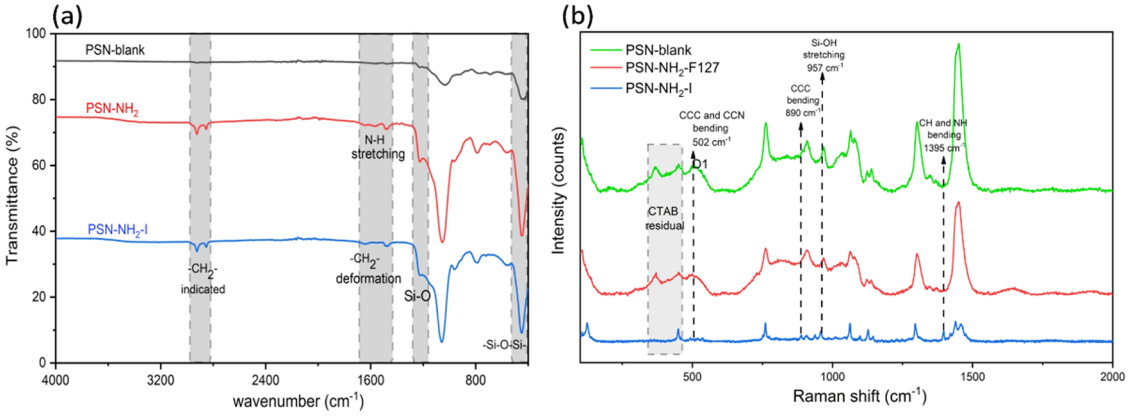

Figure 7. (a) PSN samples evaluated by FTIR spectrometry and (b) PSN samples evaluated by Raman spectrometry.

a pore expander is 2.53 nm, and after using the pore expander, it becomes 5.1 nm. With a larger pore width, PSN has the flexibility to be functionalized with amine groups. These results confirm the observations of Zhang and Li that state that porous silica nanoparticles prepared with the assistance of straight-chain alkanes, i.e., *n*-hexane, are characterized by enlarged pore diameter.[52]

Figure 5e shows the XRD pattern of PSN that is synthesized using a pore expander and those that do not use pore expander (namely, PSN calcinated). In both diffractograms, there were nonsharp peaks at 2θ angles. Thus, the use of pore expander did not result in significant changes of the crystal structure. Both of the X-ray diffraction patterns confirmed the amorphous nature of the prepared SiO_2.

Functionalization and the Effect on the Surface Properties of PSN. In the functionalization stage, variation in the volume of APTES grafted for each gram of PSN was 1.0 up to 3 APTES mL/g PSN. The amine group's functionalization was relatively successful with a fairly high (but not too high) grafting percentage obtained with the addition of APTES as much as 2.0 mL for each gram of PSN. The characterization of amine-functionalized PSN (PSN-NH_2) and blank PSN, including after adsorption of iodide ions (PSN-NH_2-I), was conducted using the sorption analysis, XRD, TEM, Fourier-transform infrared spectroscopy (FTIR), and Raman spectroscopy, as shown in Table 1, Figures 6, and 7.

Table 1 indicates that the functionalization of the amine group in PSN causes the specific surface area of PSN to decrease to about 47% smaller, while the pore volume becomes smaller than 50%. In contrast, the pore diameter is reduced by about 1 nm. After PSN-NH_2 adsorbed iodide ions, specific surface area, pore volume, and pore diameter were also significantly reduced. The decrease of PSN surface area in the presence of iodine is thought to be caused by the entry of iodine compounds into the PSN pores.

Figure 6a shows that the blank PSN isotherm curve belongs to group IV in the IUPAC classification.[48,53] Still, then after functionalization, it changes to a flatter curve, and after

https://doi.org/10.1021/acsomega.1c06492
ACS Omega 2022, 7, 13494−13506

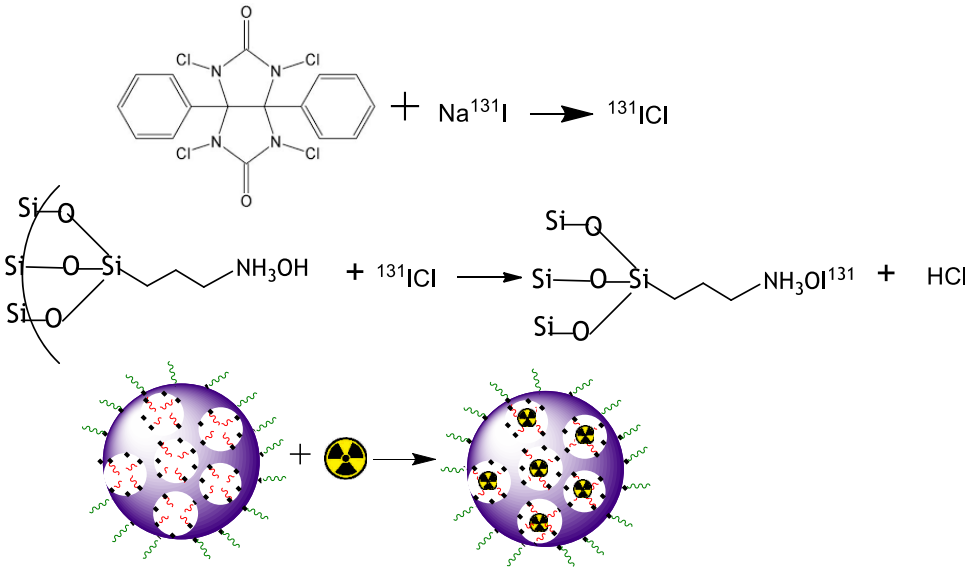

Figure 8. Mechanism of radioiodination of modified PSN using Iodogen.

adsorption of iodide ion, the isotherm curve becomes similar to that of group III in the IUPAC classification. Figure 6b,c reveals the previously porous TEM characterization of the PSN shape changes. After being functionalized with the amine group, the pore became not visible. However, the shape of the PSN still looks round. Compared with ref 54, the photograph of the functionalized PSN with the same group, namely, the amine group, looks like nonporous nanoparticles. This study also observed the effect of functionalization on nanoparticle size by TEM. Remarkably, there is no distinctive difference between the size of the PSN blank and PSN-NH_2. The sizes of both PSN and PSN-NH_2 are still around 100 nm, as observed by TEM. Figure 6d shows an X-ray diffraction pattern from PSN, which was prepared using a pore expander, and the template was removed using the extraction method (red line) and has not yet been functionalized. Then, the blue line is the PSN functionalized with the amine group. When the two patterns are compared, it is seen that the X-ray diffraction peaks of the functionalized PSN appear broadened and with decreased intensity, but can still be referred to as PSN-like nanostructures. The broadening of the diffraction peaks can be attributed to PSN pores filled with amine groups from APTES.

The FTIR spectrograms revealed differences between the blank PSN and PSN-NH_2, as shown in Figure 7a. In the PSN-NH_2, there is absorption at 1566.2 cm^{-1}, whereas the first PSN does not exist. This shows that in the blank PSN there is no amine group that binds to the OH group of PSN. In the infrared spectrogram pattern on PSN-NH_2-I, there is a shift in the wavenumber from 1566.2 to 1643 cm^{-1}. This shift is presumably the amine group on PSN-NH_2 that interacts with iodine ions. Raman spectroscopy was applied to investigate the surface structures of silica nanoparticles. Figure 7b shows the result of characterization using Raman spectroscopy, which indicates that D1 bands at 495 and 502 cm^{-1} are due to CCC and CCN bending, at 867 cm^{-1} is due to CCC bending, 945 cm^{-1} is the stretching mode (Si−OH), and 1330−1410 cm^{-1} is due to CH and NH bending. Stöber silica nanoparticles have a prominent band at ∼490 cm^{-1} but no well-resolved band at ∼605 cm^{-1}. The areas below 200 cm^{-1} indicate the fingerprint area of iodide vibrations from NaI.[55−57]

Radioiodination of PSN and PSN-NH2. After preparation, including their characterization, PSN and PSN-NH_2 are processed as radiolabeled compounds, then qualified as radiopharmaceutical candidates. There are still many limitations of nanoparticle radiolabeling that need to be studied.[36,37] For example, a burden of classical radiolabeling methods is that the induction of prosthetic groups or chelating metal ions can harm nanoparticles' pharmacokinetic profile and toxicity.[58] In this study, radioiodination (radiolabeling with radioiodine) was conducted with the direct electrophilic substitution method [using an oxidizing agent, namely, iodogen (1,3,4,6-tetrachloro-3α,6α-diphenyl glycoluril)]. The radioiodination technique using oxidizing Iodogen has the advantage of not damaging the substrate to be radioiodinated. Figure 8 shows the mechanism of PSN radioiodination using Iodogen, which refers to research by Mushtaq et al.,[58] with a thin-layer chromatogram (TLC) pattern as shown in Figure S3.

The mechanism of radioiodination of PSN and PSN-NH_2 is a combination of chemisorption, hollow encapsulation, ion exchange,[58] and electrophilic substitution.[59] PSN labeled with ^{131}I is a radiopharmaceutical candidate in this study. The radioiodination reaction begins with the formation of Iodine monochloride (I-Cl) species that was assumed as oxidation reaction of iodide ion from $Na^{131}I$ with iodogen. The radiolabeled results of PSN-^{131}I are produced by electrophilic substitution with an oxidizing agent of iodogen, in which $^{131}I^+$ exchanges with H^+. The percentage of radiochemical yield (RCY) of PSN using ^{131}I with an activity of 6 mCi (222 MBq) at various reaction times is presented in Figure 9.

The highest RCY of the PSN-^{131}I was about 85%, compared with previous results by Valliant et al. and Dubost et al.[59,60] The value was almost the same as for a sample rich in fluorine (RCY value up to 85% and RCP up to 98%), and some even had a higher RCY value as shown by Jeon et al.[61]

Figure 10 shows the radioiodination result of PSN with the variation of reaction time. Using the reaction time of 2 min, the radiolabeling yield increased to 99.30 ± 0.17%. A further increase in reaction time of 3 min and 5 min had almost no effect on the subsequent radiolabeling results. The lowest value

https://doi.org/10.1021/acsomega.1c06492
ACS Omega 2022, 7, 13494−13506

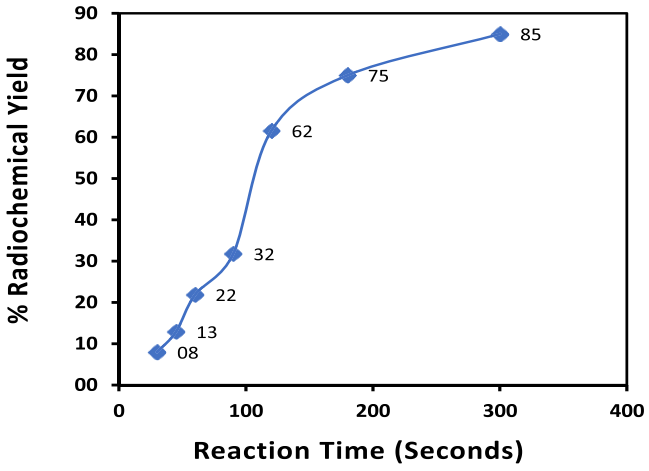

Figure 9. Percentage of radiochemical yield (RCY) of PSN using 131I with an activity of 6 mCi (222 MBq) at various reaction times.

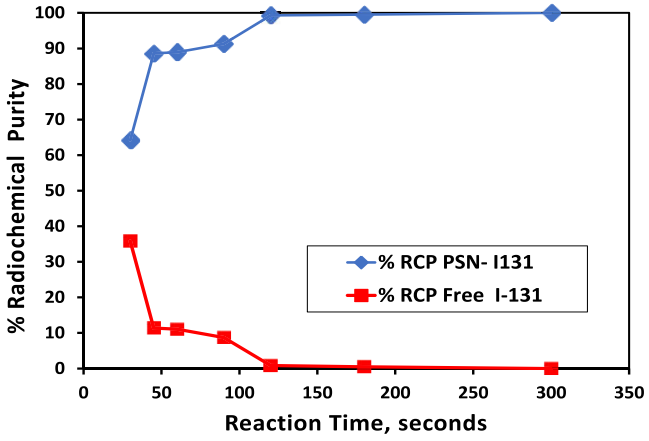

Figure 10. Radioiodination result of PSN with the variation of reaction time.

limit of RCP that is feasible for radiopharmaceuticals according to the IAEA 2018 and USP is 95%.[62,63]

Next, the study of variations PSN-to-iodogen ratio is shown in Figures 11 and S4. From three variations of ^{131}I activity of the radiolabelling, all of which could produce PSN-^{131}I with 95% RCP except in experiments with a PSN: iodogen ratio of 50:1.

Thus, it was presumed that the radiolabeling results in PSN-^{131}I have potential as a radiopharmaceutical or theranostic agent. According to IAEA 2018,[52] the activity of ^{131}I for radiotherapy can reach 2.22 GBq (approximately 60 mCi) for one fraction and 4. 44 GBq for three fractions.

Stability Test of In Vitro PSN Radioiodinated Results. The effect of time on the in vitro stability of the PSN preparation was studied to determine an appropriate time range in radiopharmaceutical preparation and to meet the criteria for quality control of radiopharmaceutical preparations as required by the IAEA.[52] Figure 12 shows a stability test for the formulation of PSN-^{131}I, which results from the radioiodination of PSN and PSN-NH_2. Data presented in Figure 12a show that the preparation of PSN-^{131}I with 12 mCi radioactivity was stable for up to 8 days in 0.05 M phosphate-buffered saline (PBS) solution, pH = 7.4.

Figure 12b shows the results of radioiodination of PSN and PSN-NH_2 and the stability test of PSN-^{131}I with variations in

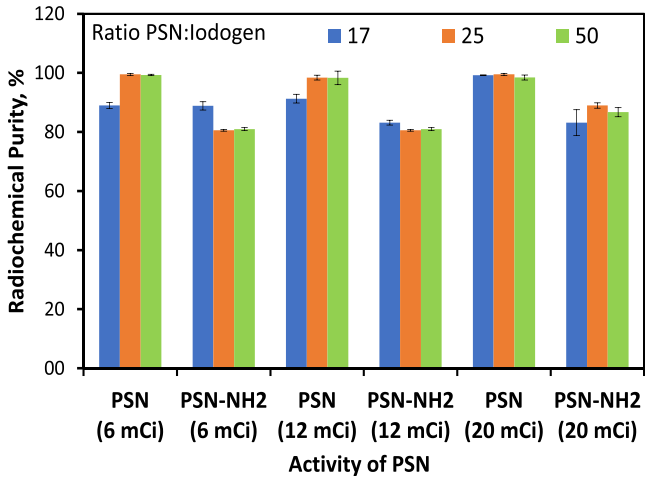

Figure 11. Radioiodination result of PSN with the variation of the radioactivity of ^{131}I and PSN:iodogen ratio.

the specific surface area. The RCP results were different by comparing the results of radiolabeling on PSNs with several PSNs with other specific surface areas. The difference in the RCP results indicates that the surface properties of the PSN influence the radiolabeling results. In this case, it can be observed that there is a correlation between the specific surface area of the PSN and the radiolabeling results.

This observation is in line with research by Mirshojaei et al, who said that multifunctional nanoparticles have large surface areas, where multiple functional moieties can be incorporated, including ligands for site-specific targeting and radionuclides.[64] Figure 12c shows that the preparation of PSN-^{131}I with 12 mCi radioactivity is stable for up to 8 days in bovine serum albumin (BSA) medium. Figure 12d also shows that the preparation of PSN-^{131}I with 12 mCi radioactivity is stable for up to 8 days in human serum albumin (HSA). When it comes to the half-life, the stability of the compound labeled PSN-^{131}I has a tendency to the physical half-life of radionuclide ^{131}I which is 8 days. It is estimated that the PSN-^{131}I radiopharmaceutical could be injected without precautions of byproducts because of the radiolysis of PSN-^{131}I in PBS, BSA, and HSA medium.

The stability test is in line with the suggestion of IAEA 2018[52] that validation and stability studies should be carried out at the highest radioactive concentrations used in clinics or hospitals to demonstrate the "worst possible" effect of radiolysis on radiopharmaceutical stability.

Cytotoxicity and Cellular Uptake of PSN. As a potential drug vehicle candidate, the synthesized PSN was tested for cytotoxicity against a sample of normal cell lines such as 3T3-J2 Cell Line—Embryonic mouse fibroblasts as presented in Figure 13a. The cellular uptake of PSN^{131}I labeled compound was tested in cancer cell lines such as prostate cancer cells, namely, RM1 and LNCaP cell lines as shown in Figure 13b.

Cytotoxicity tests have been carried out at 1 μg/mL to 1250 μg/mL concentrations of PSN in PBS/F-127 solutions. In this investigation, normal 3T3 fibroblast cell lines were used with a total of 1×10^4 cells. Relationship between the test PSN and PSN-NH_2 concentration (μg/mL) and cell viability (%) after 24 h exposure using the 3-(4,5-dimethylthiazol-2-yl)-2,5-diphenyltetrazolium bromide (MTT) assay.

The half-maximal inhibitory concentration (IC_{50}) for PSN is 150 μg/mL, while for PSN-NH_2, it is 170 μg/mL. It was observed that PSN is nontoxic at 1−150 μg/mL till 24 h while

https://doi.org/10.1021/acsomega.1c06492
ACS Omega 2022, 7, 13494−13506

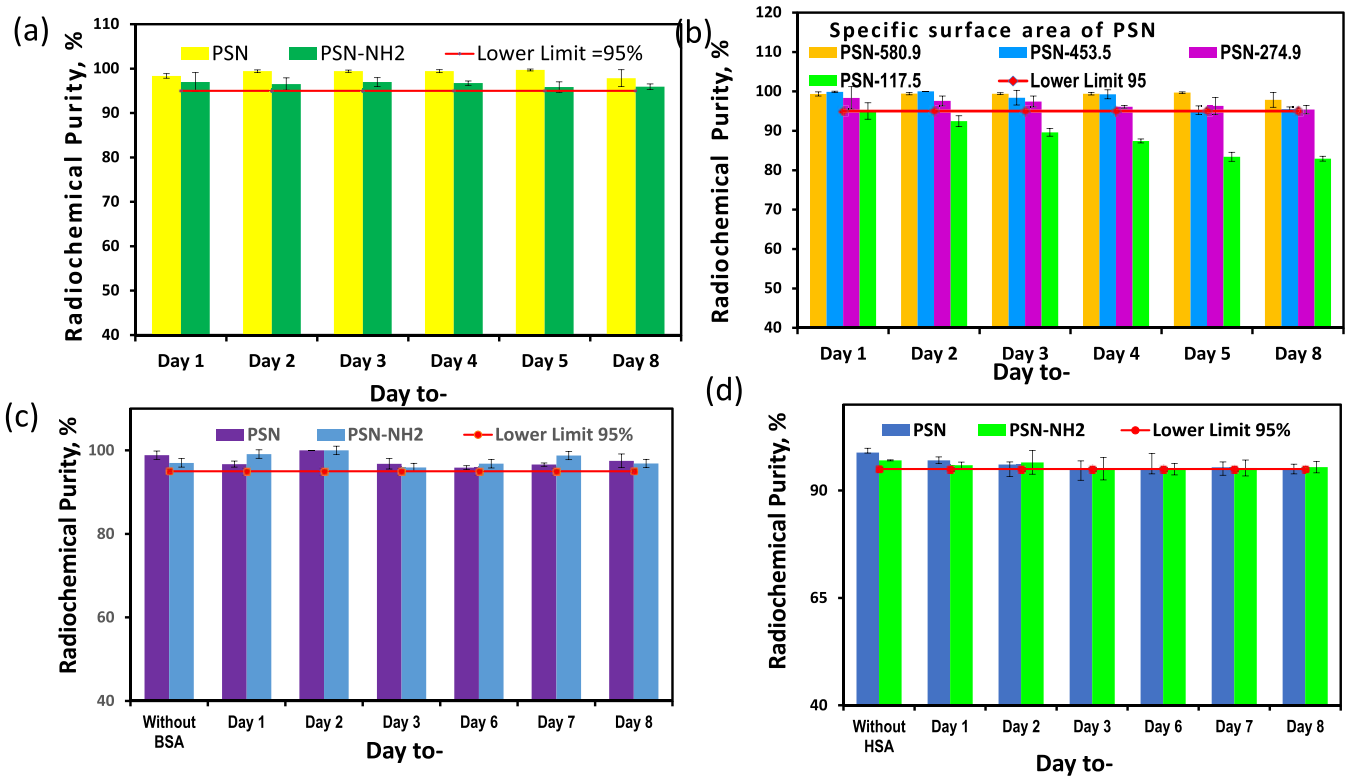

Figure 12. Stability test of PSN-^{131}I, which is the result of radioiodination of PSN and PSN-NH_2: (a) Stability test of PSN-^{131}I in 0.05 M phosphate buffer saline (PBS) solution, pH = 7.4; (b) stability test of PSN-^{131}I with variations in specific surface area in 0.05 M PBS solution, pH = 7.4; (c) stability test of PSN-^{131}I in bovine serum albumin (BSA); and (d) stability test of PSN-^{131}I in human serum albumin (HSA).

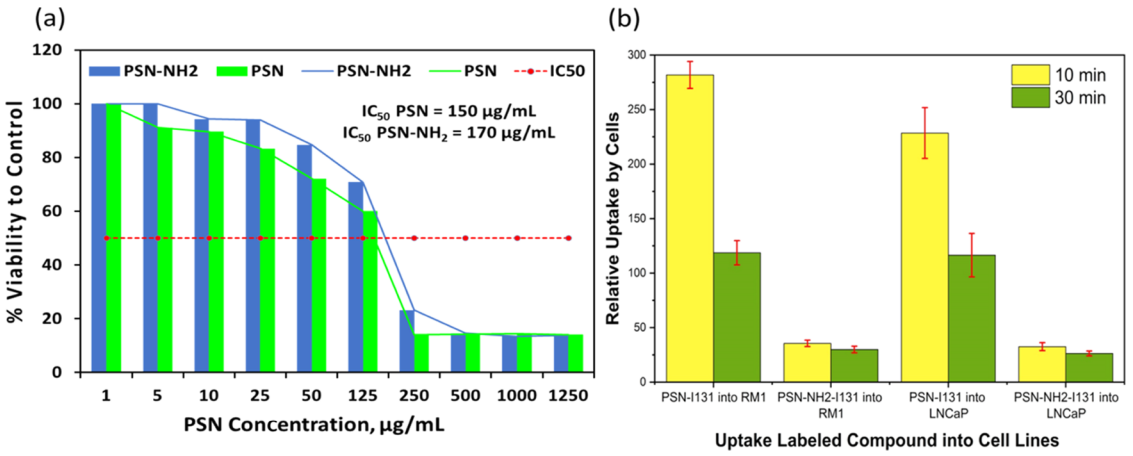

Figure 13. (a) Cytotoxicity of PSN and PSN-NH_2 into 3T3-J2 Cell Line—Embryonic mouse fibroblasts and (b) cellular uptake of PSN-^{131}I and PSN-NH_2-^{131}I into prostate cancer cell lines such as RM1 and LNCaP cancer cell lines.

PSN-NH_2 is nontoxic at 1−170 μg/mL till 24 h. However, from Figure 13a, it can be seen that the presence of an amine group on PSN can slightly reduce the cytotoxicity into 3T3 cells. The results of the study are quite encouraging compared to studies conducted by previous researchers. For example, Mateo et al. carried out the same test on fibroblast cells with gold nanoparticles (AuNP) whose highest IC50 value was 19.3 μg/mL.[65] Meanwhile, Dechsakulthorn reported the IC_{50} values of zinc oxide (ZnO) and titanium dioxide (TiO_2) nanoparticles. At 24 h exposure, the IC_{50} value of ZnO was 49.56 ± 12.89 ppm and that of TiO_2 was 2696 ± 667 ppm.[66]

Internalization and accumulation of radioactive drugs into cancer cells are critical for the therapeutic effect against cancer itself.[67] Cellular uptake experiments in vitro can represent those characteristics for prospective drug vehicles. In this study, a cellular uptake experiment of a drug candidate in the form of a compound labeled ^{131}I has been carried out in prostate cancer cell lines, i.e., RM1 and LNCaP cell lines, as shown in Figure 13b.

From the initial experimental data, the results were unexpected in the first 10 min of observing the cellular uptake of PSN-^{131}I into the RM1 cell line. The calculated uptake percentage of the initial PSN-^{131}I reached a value of more than 90% at 10 min and slightly more than 60% at 30 min (see Supporting Information Figure S5). Meanwhile, the uptake of PSN-NH_2-^{131}I was more than 10% into the RM1 cell line and

https://doi.org/10.1021/acsomega.1c06492
ACS Omega 2022, 7, 13494−13506

between 6 and 10% into the LNCaP cell line at 10 and 30 min, respectively. Figure 13b shows the relative value of uptake normalized to the activity of compound I-131 only.

It can be seen that PSN-^{131}I reached a value of more than 200 times while PSN-NH_2-^{131}I reached a value of 30 times. The value of cellular uptake is relatively high compared to research by several scientists.[68,69] Thus, it can be temporarily stated that the compounds labeled PSN-^{131}I and PSN-NH_2-^{131}I have good cellular uptake capabilities, so they are suitable as candidates for radioactive drug vehicles.

Comparative Study of Several Related Literature and Characterization. Table 2 shows the results of the radiolabeling of several nanoparticles, which are relatively feasible compared to the results of the PSN radiolabeling.[70−73] One of the reasons is that the RCY and RCP yields of radioiodinated PSN and PSN-NH_2 are relatively high and stable. This study is still relatively new, and it is still rare to find similar research on silica nanoparticles. In addition, the labeled compound produced was stable and not radiolyzed until the half-life of ^{131}I. The cytotoxicity and cellular uptake results of PSN and PSN-NH_2 show potential and promising results.

CONCLUSIONS AND OUTLOOK

In this work, we have succeeded in preparing PSN using a combination of the Stöber method and liquid crystal templating with TEA-F127 as a dispersant or steric stabilizer for PSN and an organic *n*-hexane solution as a pore expander. The satisfactory result of achievable PSN size was 100−150 nm with a PDI of 0.24 at a minimum of 30 min of sonication time and a TEA-F127:CTAB ratio of 7.5 mL/g. This implies that PSN can reach cancer cell targets using the EPR principle as a drug vehicle. Favorably, the PSN pore diameter changed from the usual 2−3 to 5.1 nm in the PSN synthesis using *n*-hexane as a pore expander. The widening of the pore diameter is advantageous because it provides flexibility for the functionalization of the amine group. The ζ-potential of the PSN is −37.4 to −20.8 mV, which correlates with moderate stability to incipient instability. This PSN can be appropriately functionalized using an amine precursor, APTES, which aims to direct the properties of PSN-NH_2 so that it is biocompatible. At the radiolabeling stage, it can be concluded that there is no significant difference between the two types of materials of PSN and PSN-NH_2. In both materials, the radiolabeling can achieve more than 95% RCP values. The RCP results are different by comparing the results of radiolabeling on PSNs with several PSNs with other specific surface areas. The difference in the RCP results indicates that the surface properties of the PSN influence the radiolabeling results. The two prospective radiopharmaceuticals produced, both PSN-^{131}I and PSN-NH_2-^{131}I, had relatively the same in vitro stability properties in a 0.05 M PBS pH 7.4, saline, BSA, and HSA medium, which lasted up to 8 days. Both PSN-^{131}I and PSN-NH_2-I were still stable when examined at 12 mCi activity, indicating that radiolysis did not occur. The results of the cytotoxicity test on fibroblasts cells (3T3 Line) showed that it was not toxic up to a concentration of 150 μg/mL for PSN and 170 μg/mL for PSN-NH_2. It can be seen that the labeled compound of PSN-^{131}I reached a value of more than 200 times, while PSN-NH_2-^{131}I reached a value of 30 times. Thus, we can conclude that PSN and PSN-NH_2 are potential candidates as iodine-131 (^{131}I) drugs vehicles because their size and surface properties could be controlled; furthermore, they can be radiolabeled. This study is still very possible

Table 2. Literature Reviews Regarding Radiolabeling of Nanoparticles[61,67,68,71−74]

researcher name, title, and year of publication	radioactivity and stability	results
Chrastina and Schnitzer;[73] iodine-125 radiolabeling of silver nanoparticles for in vivo SPECT imaging	0.4−0.6 μCi/μg of 125I-AgNPs; no stability data	RCY > 80%
Jeon et al.;[61] an optimized protocol for the efficient radiolabeling of gold nanoparticles using a 125I-labeled azide prosthetic group	150 MBq no stability data	radiochemical yield (75 ± 10%, n = 8) and RCP ≥ 99%
Zhang et al.;[72] synthesis and bioevaluation of iodine-131 directly labeled cyclic RGD-PEGylated gold nanorods for tumor-targeted imaging	stability in vitro with RCP of 97.79 ± 0.50% in PBS and 95.59 ± 0.73% in FBS at 48 h	RCY [^{131}I]GNR-PEG-cRGD = 64.54 ± 3.81%, RCP 98.17 ± 0.86%
Walsh;[71] chemisorption of iodine-125 to gold nanoparticles allows for real-time quantitation and potential use in nanomedicine	in three different buffers for >100 days at 5 °C, >92%; 20 μCi	RCP > 92%
Aries et al.;[70] iodogen method on iodine-131 (^{131}I) radiolabelling of silver nanoparticle (AgNPs) as a new agent of molecular imaging	5 days in room temperature RCP > 90%	RCP 94.5 ± 0.21%
Mohammadi et al.;[68] cellular uptake, imaging, and pathotoxicological studies of novel Gd[III]-DO3A-butrol nanoformulation		the concentration limit of the noncytotoxic nanoformulation is 2 × 5 μg/mL and cellular uptake is 70%
Piccolo et al.;[67] exploring cellular uptake, accumulation, and mechanism of action of a cationic Ru-based nanosystem in human preclinical models of breast cancer		the highest cellular uptake is 80%
Xie et al.;[74] ^{131}I-IITM and 211At-AITM: two novel small-molecule radiopharmaceuticals targeting oncoprotein metabotropic glutamate receptor 1	RCY 42.7% stability >97% at 24 h	the highest cellular uptake is 50−60%

https://doi.org/10.1021/acsomega.1c06492
ACS Omega 2022, 7, 13494−13506

because we are still doing follow-up research that attributes to this topic.

MATERIALS AND METHODS

Materials. The materials used to prepare the modified PSN are silica precursors such as tetraethyl orthosilicate (TEOS), surfactant cetyltrimethylammonium bromide (CTAB) as a pore-forming template, triethanolamine (TEA, as growth inhibitor of nanoparticle nucleus), Pluronic F-127 are triblock copolymers consisting of PEG (PPO−PEO) blocks-PPO as dispersant and substitute for PEG-silane compounds. Other reagents are NH4OH 25%, HCl 36%, NaOH crystals, *n*-hexane, absolute ethanol, and 3-aminopropyltriethoxysilane (APTES). The materials used for radiolabeling the PSN-NH_2 were crystalline NaI, iodogen (1,3,4,6-tetrachloro-3,6-diphenylglycouril), 0.9% biological saline (NaCl), Whatman paper 31ET, ITLC-SA, universal pH indicator, phosphate buffer solution pH 7.4, chloroform, methanol, and distilled water. All chemicals were of p.a. grade from Merck, Sigma-Aldrich, and Fluka. Solution 131I is produced in the multipurpose reactor G.A. Siwabessy with a neutron flux of 1015 neutrons/cm^2·s. The target used is a natural TeO2 compound. The specific activity of 131I produced was 0.7 Ci/mL.

Preparation of Modified Porous Silica Nanoparticles. In principle, PSN was prepared by a combination of the Stöber and the templating liquid crystal method as follows. CTAB (1.0 g) was dissolved in 160 mL of water, stirred, and then added 4 mL of ammonia solution, and a 7.5 mL solution of 1 g of F127 in 7.5 mL of TEA, and then stirred until the mixture was completely dissolved. To the solution, a mixture of solutions containing 20 mL of *n*-hexane (as pore-expanding agent) and 5 mL of TEOS was added dropwise for 30 min. The stirring or agitation reaction was continued at 35 °C for 12 h with a stirring speed of 200 rpm. After the white colloid is produced, the precipitate is filtered or centrifuged and decanted with ethanol−HCl (0.1%). The extraction was repeated up to six times, and the residue was freeze-dried.

Functionalization of Porous Silica Nanoparticles. The amine functionalization was carried out using the glass apparatus for reflux by the postsynthesis grafting method. PSN (10 g) was dispersed into 150 mL of toluene and 3.2 mL of water and stirred for 1 h to form surface hydration. A total of APTES (approximately equivalent to one monolayer silane/nm^2) was added to the mixture and refluxed for 4 h at 75 °C. After that, the mixture was distilled and cooled at room temperature. The modified material was washed with isopropyl alcohol solution and dried. Studies on the influential parameters were carried out by experiments on variations in the number of APTES. FTIR and TEM characterization of amines grafted on PSN was performed.

Radioiodination of PSN. Radioiodination of PSN was conducted using an oxidizing agent such as iodogen. Iodogen (2 mg) was dissolved in 1 mL of chloroform, transferred to glass tubes, and stirred. The chloroform was evaporated by dry N_2 gas, and iodogen was deposited on the glass tube wall as a thin film. A certain amount (in milligrams) of PSN or PSN-NH_2 is dispersed in 40 mL of distilled water and sonicated for 30 min. The particulate suspension of nanoparticles is measured using a particle size analyzer−dynamic light scattering (PSA−DLS). Then, 1 mL of the remaining particulates was transferred to iodogen-containing glass tubes, added 400 mL of phosphate buffer, and stirred for 30 s. Then, 50 mL of radioactive compound ^{131}I with particular radioactivity (depending on the radioactivity variation) was added to the suspension, followed by the addition of a 0.05 N phosphate buffer solution, and stirred again for about 1−5 min (depending on the variation times). The particulate suspension was centrifuged for 10 min at a rotation rate of 8000 rpm and decantated three times. The RCP was determined by calculating the radioactivity by paper chromatography using a TLC scanner. An example of a chromatogram showing radiolabeling results in TLC with the RF of free ^{131}I and PSN-^{131}I is given. The radiochemical purity yield is calculated as in eqs1 and 2.

$$\%\mathrm{RCP} = \frac{\text{count in the RF region}}{\text{total count}} \times 100\% \quad (1)$$

$$\%\text{RC impurities} = \frac{\text{count in the RF region} - 100}{\text{total count}} \times 100\% \quad (2)$$

These radioiodinated compounds were measured using radiochemical yield (RCY, the amount of activity in the isolated product expressed as a percentage of initial radioactivity or isolated) and radiochemical purity (RCP, the percentage of radionuclide activity to the total activity of all radionuclides in the sample). RCY is determined by a dose calibrator, while RCP uses a radioactive thin-layer chromatography (TLC) scanner. Determination of radiochemical purity percentage is based on the separation of PSN-^{131}I from ^{131}I impurity-free (not bound by PSN) using Whatman 1 M paper chromatography as the stationary phase and a 75% mobile-phase methanol solution. The free ^{131}I impurities will also rise with this chromatographic system, carried by the 75% methanol solution eluent, while the radioiodination results will remain in the zero phase.

Characterization. The particle size analyzer−dynamic light scattering (PSA−DLS) technique with a Horiba SZ-100 was used to characterize PSN with nanoparticle size, polydispersity index (PDI), and ζ-potential. The adsorption properties of porous silica nanoparticles against N_2 gas were observed by the Brunauer−Emmett−Teller (BET) method using the Quantachrome Novoid surface area analysis (NOVA 2000) instrument. TEM characteristics were observed with a JEOL transmission electron microscope (TEM) operating at 100/120 kV with LaB6. A Bruker α II FTIR spectrometer is used to characterize nonporous silica nanoparticles and functionalized porous silica nanoparticles. The wavenumber scan was carried out at 400−4000 cm^{-1}. Raman spectra were recorded using a Horiba Scientific device (France) in the range of 100−2000 cm^{-1}.

Cellular Uptake Study. The prostate cancer cell line RM1 was purchased from Elabscience (Wuhan, China), and LNCaP cell line was bought from ECACC (Salisbury, United Kingdom). The RM1 and LNCaP cell line (5.0×10^5 cells/well) was preincubated in a 24-well culture plate overnight. After preincubation, the culture medium was removed, and the cells were washed with Hank's balanced salt solution (HBSS). Then, the cells were incubated with PSN-I^{131}, PSN-NH_2-I^{131}, and I-131 in HBSS at 37 °C for 10, 30, and 60 min. Subsequently, the cells were washed with HBSS and lysed using NaOH 0.2 M. The cell lysate was counted by a well-type automatic γ counter (2470 Wizard2, PerkinElmer).

Toxicity of Porous Silica Nanoparticle to 3T3 Cells. The cytotoxicities of PSN-NH2 and PSN were determined using the MTT assay. The mouse embryonic fibroblast 3T3-L1

https://doi.org/10.1021/acsomega.1c06492
ACS Omega 2022, 7, 13494−13506

cell line (ATCC CL-173) was preincubated in a 96-well culture plate overnight at 37 °C. Therefore, the cells were cultured in addition to 1250, 1000, 500, 250, 125, 50, 10, 5, and 1 μg/mL of PSN-NH2 and PSN for 24 h. The cells cultured without any treatment were used as a negative control. After the incubation, the thiazolyl blue tetrazolium bromide reagent (Sigma-Aldrich, Cat. no. M2128) was added directly and the cultured cells were incubated at 37 °C for 120 min. The absorbance in each well was determined using a microplate spectrophotometer in the wavelength range of 550−600 nm. The cell viability was then measured as a percentage of cell viability compared to the negative control.

■ ASSOCIATED CONTENT

Supporting Information

The Supporting Information is available free of charge at https://pubs.acs.org/doi/10.1021/acsomega.1c06492.

Additional data on DLS, TEM, chromatogram, radioiodination, and cellular uptake (PDF)

■ AUTHOR INFORMATION

Corresponding Author

Imam Prasetyo − *Department of Chemical Engineering, Faculty of Engineering, Universitas Gadjah Mada, Yogyakarta 55281, Indonesia;* orcid.org/0000-0003-3912-4919; Email: imampras@ugm.ac.id

Authors

Maria Christina Prihatiningsih − *Department of Chemical Engineering, Faculty of Engineering, Universitas Gadjah Mada, Yogyakarta 55281, Indonesia; Polytechnic Institute of Nuclear Technology, National Research and Innovation Agency, Yogyakarta 55281, Indonesia;* orcid.org/0000-0002-9614-6754

Teguh Ariyanto − *Department of Chemical Engineering, Faculty of Engineering, Universitas Gadjah Mada, Yogyakarta 55281, Indonesia;* orcid.org/0000-0002-9454-9541

Edy Giri Rachman Putra − *Center for Science and Technology of Advanced Materials, National Research and Innovation Agency, Banten 15314, Indonesia*

Veronika Yulianti Susilo − *Research and Technology Center for Radioisotope and Radiopharmaceutical, National Research and Innovation Agency, Banten 15314, Indonesia*

Isa Mahendra − *Research and Technology Center for Applied Nuclear, National Research and Innovation Agency, Bandung 40132 West Java, Indonesia*

Complete contact information is available at: https://pubs.acs.org/10.1021/acsomega.1c06492

Author Contributions

The manuscript was written through contributions of all authors. All authors have given approval to the final version of the manuscript.

Notes

The authors declare no competing financial interest.

■ ACKNOWLEDGMENTS

This research was funded by Grant of Rekognisi Tugas Akhir, Universitas Gadjah Mada, Indonesia, grant number 3143/UN1.P.III/DIT-LIT/PT/2021. The authors thank Center for Radioisotope and Radiopharmaceutical Technology for Radioisotope of the Nuclear Technology Research Organization−National Research and Innovation Agency Indonesia. They also thank G.A. Siwabessy Multipurpose Reactor-National Research and Innovation Agency, Indonesia.

■ REFERENCES

(1) Moeendarbari, S.; Tekade, R.; Mulgaonkar, A.; Christensen, P.; Ramezani, S.; Hassan, G.; Jiang, R.; Orhan, K. Ö. z.; Hao, Y.; Sun, X. Theranostic Nanoseeds for Efficacious Internal Radiation Therapy of Unresectable Solid Tumors. *Sci. Rep.* **2016**, *6*, No. 20614.

(2) Elgqvist, J. Nanoparticles as Theranostic Vehicles in Experimental and Clinical Applications—Focus on Prostate and Breast Cancer. *Int. J. Mol. Sci.* **2017**, *18*, No. 1102.

(3) Feng, Y.; Panwar, N.; Tnga, D. J. H.; Tjina, S. C.; Wangb, K.; Yonga, K. The application of mesoporous silica nanoparticle family in cancer theranostics. *Coord. Chem. Rev.* **2016**, *319*, 86−109.

(4) Rösch, F.; Herzog, H.; Qaim, S. M. The Beginning and Development of the Theranostic Approach in Nuclear Medicine, as Exemplified by the Radionuclide Pair 86Y and 90Y. *Pharmaceuticals* **2017**, *10*, No. 56.

(5) Shetty, Y.; Prabhu, P.; Prabhakar, B. Emerging vistas in theranostic medicine. *Int. J. Pharm.* **2019**, *558*, 29−42.

(6) Donya, M.; Radford, M.; Elguindy, A.; Firmin, D.; Yacoub, M. Review article Radiation in medicine: Origins, risks and aspirations. *Glob. Cardiol. Sci. Pract.* **2014**, *57*, 437−448.

(7) Yordanova, A.; Eppard, E.; Kürpig, S.; Bundschuh, R. A.; Schönberger, S.; Gonzalez-Carmona, M.; Feldmann, G.; Ahmadzadehfar, H.; Essler, M. Theranostics in nuclear medicine practice. *OncoTargets Ther.* **2017**, *10*, 4821−4828.

(8) Sheng, J.; Wang, X.; Yan, J.; Pan, D.; Yang, R.; Wang, L.; Xub, Y.; Yang, M. Theranostic radioiodine-labelled melanin nanoparticles inspired by clinical brachytherapy seeds. *J. Mater. Chem. B* **2018**, *6*, 8163−8169.

(9) Nagarajah, J.; Janssen, M.; Hetkamp, P.; Jentzen, W. Iodine symporter targeting with 124I/131I theranostics. *J. Nucl. Med.* **2017**, *58*, 34S−38S.

(10) Martins, P. A.; da Silva, J. L.; Ramos, M. P. S.; de Oliveira, I. M.; Felgueiras, C. F.; Herrerias, R.; Zapparoli, J. C. L.; Mengatti, J.; Fukumori, N. T. O.; Matsuda, M. In *Radiochemical Stability of Radiopharmaceutical Preparations*, 2011 International Nuclear Atlantic Conference—INAC 2011, Belo Horizonte, MG, Brazil, Oct 24−28, 2011.

(11) Okamoto, S.; Shiga, T.; Tamaki, N. Clinical Perspectives of Theranostics. *Molecules* **2021**, *26*, No. 2232.

(12) Sgouros, G.; Bodei, L.; McDevitt, M. R.; Nedrow, J. Radiopharmaceutical therapy in cancer: clinical advances and challenges. *Nat. Rev. Drug Discovery* **2020**, *19*, 589−608.

(13) Wang, L. Z.; Lim, T. L.; Padakanti, P. K.; Carlin, S. D.; Alavi, A.; Mach, R. H.; Prud'homme, R. Kinetics of Nanoparticle Radiolabeling of Metalloporphyrin with 64Cu for Positron Emission Tomography (PET) Imaging. *Ind. Eng. Chem. Res.* **2020**, *59*, 19126−19132.

(14) Wyszomirska, A. Iodine-131 for therapy of thyroid diseases. Physical and biological basis. *Nucl. Med. Rev.* **2012**, *15*, 120−123.

(15) Kitahara, C. M.; de Gonzalez, A. B.; Bouville, A.; Brill, A. B.; Doody, M. M.; Melo, D. R.; Simon, S. L.; Sosa, J. A.; Tulchinsky, M.; Villoing, D.; Preston, D. L. Association of Radioactive Iodine Treatment with Cancer Mortality in Patients with Hyperthyroidism. *JAMA Intern. Med.* **2019**, *179*, 1034−1042.

(16) Kang, H. J.; Lee, S.; Byun, B. H.; Kim, K. M.; Lim, I.; Choi, C. W.; Suh, C.; Kim, W. S.; Nam, S.; Lee, S. I.; Eom, H. S.; Shin, D.; Lim, S. M. Repeated radioimmunotherapy with 131I-rituximab for patients with low-grade and aggressive relapsed or refractory B cell non-Hodgkin lymphoma. *Cancer Chemother. Pharmacol.* **2013**, *71*, 945−953.

(17) Kim, E.; Ko, H. Y.; Yu, A. R.; Kim, H.; Zaheer, J.; Kang, H. J.; Lim, Y.; Cho, K. D.; Joo, H.; Kang, M. K.; et al. Inhibition of HIF-1α

by Atorvastatin during131I-RTX Therapy in Burkitt's Lymphoma Model. *Cancers* **2020**, *12*, 1−25.
(18) Xu, X.; Li, M.; Hu, J.; Chen, Z.; Yu, J.; Dong, Y.; Sun, C.; Han, J. Somatic mitochondrial DNA D - loop mutations in meningioma discovered: A preliminary data A comprehensive overview of mitochondrial DNA 4977-bp. *J. Cancer Res. Ther.* **2018**, *14*, 1525−1534.
(19) Kositwattanarerk, A.; Changmuang, W.; Sangsuriyan, J.; Thongklam, K.; Sritara, C.; Utamakul, C.; Chamroonrat, W.; Thamnirat, K.; Anongpomyochkul, Y.; Chancharunee, S. 131I-Rituximab Treatment in Patient with Relapsed Non-Hodgkin's Lymphoma: The First Case Report in Thailand. *J. Med. Assoc. Thailand* **2013**, *96*, 756−760.
(20) Anongpornjossakul, Y.; Sriwatcharina, W.; Thamnirata, K.; Chamroonrata, W.; Kositwattanarerka, A.; Utamakula, C.; Sritaraa, C.; Chokesuwattanasakula, P.; Thokanitb, N. S.; Pakakasamac, S.; et al. Iodine-131 metaiodobenzylguanidine (131I-mIBG) treatment in relapsed/refractory neuroblastoma. *Nucl. Med. Commun.* **2020**, *41*, 336−343.
(21) Rubio, P. M.; Galán, V.; Rodado, S.; Plaza, D.; Martínez, L. MIBG Therapy for Neuroblastoma: Precision Achieved With Dosimetry, and Concern for False Responders. *Front. Med.* **2020**, *7*, No. 173.
(22) Furtado, R. V.; Ha, L.; Clarke, S.; Sandroussi, C. Adjuvant Iodine131 Lipiodol after Resection of Hepatocellular Carcinoma. *J. Oncol.* **2015**, *2015*, No. 746917.
(23) D'Huyvetter, M.; De Vos, J.; Caveliers, V.; Vaneycken, I.; Heemskerk, J.; Duhoux, F. P.; Fontaine, C.; Vanhoeij, M.; Windhorst, A. D.; van der Aa, F.; et al. Phase I Trial of 131I-GMIB-Anti-HER2-VHH1, a New Promising Candidate for HER2-Targeted Radionuclide Therapy in Breast Cancer Patients. *J. Nucl. Med.* **2021**, *62*, 1097−1105.
(24) Kanikowski, M.; Skowronek, J.; Kubaszewska, M.; Chicheł, A.; Milecki, P. Permanent implants in treatment of prostate cancer. *Rep. Pract. Oncol. Radiother.* **2008**, *13*, 150−167.
(25) Ghaferi, M.; Koohi Moftakhari Esfahani, M..; Raza, A.; Al Harthi, S.; Ebrahimi Shahmabadi, H.; Alavi, S. E. *Mesoporous Silica Nanoparticles: Synthesis Methods and Their Therapeutic Use-Recent Advances*; Taylor & Francis, 2021; Vol. *29*.
(26) Bavandpour, A. K.; Bakhshi, B.; Najar-peerayeh, S. The roles of mesoporous silica and carbon nanoparticles in antigen stability and intensity of immune response against recombinant subunit B of cholera toxin in a rabbit animal model. *Int. J. Pharm.* **2020**, *573*, No. 118868.
(27) Morsi, R. E.; Mohamed, R. S. Nanostructured mesoporous silica: influence of the preparation conditions on the physical-surface properties for efficient organic dye uptake. *R. Soc. Open Sci.* **2018**, *5*, No. 172021.
(28) Pu, X.; Li, J.; Qiao, P.; Li, M.; Wang, H.; Zong, L.; Yuan, Q.; Duan, S. Mesoporous Silica Nanoparticles as a Prospective and Promising Approach for Drug Delivery and Biomedical Applications. *Curr. Cancer Drug Targets* **2019**, *19*, 285−295.
(29) Li, T.; Shi, S.; Goel, S.; Shen, X.; Xie, X.; Chen, Z.; Zhang, H.; Li, S.; Qin, X.; Yang, H.; Wu, C.; Liu, Y. Recent advancements in mesoporous silica nanoparticles towards therapeutic applications for cancer. *Acta Biomater.* **2019**, *89*, 1−13.
(30) Croissant, J. G.; Butler, K. S.; Zink, J. I.; Brinker, C. J. Synthetic amorphous silica nanoparticles: toxicity, biomedical and environmental implications. *Nat. Rev. Mater.* **2020**, *5*, 886−909.
(31) Food and Drug Administration (FDA). CFR Code of Federal Regulations Title 21 The information on this page is current as of April 1 2016. In *WwwFdaGov*; FDA, 2019; Vol. *721*, pp 1−10. https://www.accessdata.fda.gov/scripts/cdrh/cfdocs/cfCFR/CFRSearch.cfm?fr=170.3&SearchTerm=170.3.
(32) Yildirim, A.; Demirel, G. B.; Erdem, R.; Senturk, B.; Tekinay, T.; Bayindir, M. Pluronic polymer capped biocompatible mesoporous silica nanocarriers. *Chem. Commun.* **2013**, *49*, 9782−9784.
(33) Watermann, A.; Brieger, J. Mesoporous Silica Nanoparticles as Drug Delivery Vehicles in Cancer. *Nanomaterials* **2017**, *7*, No. 189.
(34) Jafari, S.; Derakhshankhah, H.; Alaei, L.; Fattahi, A.; Varnamkhastia, B. S.; Ali Akbar Saboury, A. A. Mesoporous silica nanoparticles for therapeutic/diagnostic applications. *Biomed. Pharmacother.* **2019**, *109*, 1100−1111.
(35) Narayan, R.; Nayak, U. Y.; Raichur, A. M.; Gang, S. Mesoporous silica nanoparticles: A comprehensive review on synthesis and recent advances. *Pharmaceutics* **2018**, *10*, No. 118.
(36) Pellico, J.; Gawne, P. J.; de Rosales, R. T. M. Radiolabelling of nanomaterials for medical imaging and therapy. *Chem. Soc. Rev.* **2021**, *50*, 3355−3423.
(37) Lamb, J.; Holland, J. P. Advanced methods for radiolabeling multimodality nanomedicines for SPECT/MRI and PET/MRI. *J. Nucl. Med.* **2018**, *59*, 382−389.
(38) Peer, D.; Karp, J. M.; Hong, S.; Farokhzad, O. C.; Margalit, R.; Langer, R. Nanocarriers as an emerging platform for cancer therapy. *Nat. Nanotechnol.* **2007**, *2*, 751−760.
(39) Nakamura, Y.; Mochida, A.; Choyke, P. L.; Kobayashi, H. Nanodrug Delivery: Is the Enhanced Permeability and Retention Effect Sufficient for Curing Cancer? *Bioconjugate Chem.* **2016**, *27*, 2225−2238.
(40) Stöber, W.; Fink, A.; Bohn, E. Controlled Growth of Monodisperse Silica Spheres in the Micron Size Range. *J. Colloid Interface Sci.* **1968**, *26*, 62−69.
(41) Yismaw, S.; Kohns, R.; Schneider, D.; Poppitz, D.; Ebbinghaus, S. G.; Gläser, R.; Tallarek, U.; Enke, D. Particle size control of monodispersed spherical nanoparticles with MCM-48-type mesostructure via novel rapid synthesis procedure. *J. Nanopart. Res.* **2019**, *21*, No. 258.
(42) Beltrán-Osuna, Á. A.; Perilla, J. E. Colloidal and spherical mesoporous silica particles: synthesis and new technologies for delivery applications. *J. Sol-Gel Sci. Technol.* **2016**, *77*, 480−496.
(43) Rahmani, S.; Budimir, J.; Sejalon, M.; Daurat, M.; Aggad, D.; Vivès, E.; Raehm, L.; Garcia, M.; Lichon, L.; Gary-Bobo, M.; Durand, J. O.; Charnay, C. Large pore mesoporous silica and organosilica nanoparticles for pepstatin A delivery in breast cancer cells. *Molecules* **2019**, *24*, No. 332.
(44) Wu, S. H.; Mou, C. Y.; Lin, H. Synthesis of mesoporous silica nanoparticles. *Chem. Soc. Rev.* **2013**, *42*, 3862−3875.
(45) Ikari, K.; Suzuki, K.; Imai, H. Structural control of mesoporous silica nanoparticles in a binary surfactant system. *Langmuir* **2006**, *22*, 802−806.
(46) Niculescu, V. C. Mesoporous Silica Nanoparticles for Bio-Applications. *Front. Mater.* **2020**, *7*, No. 36.
(47) Swar, S.; Máková, V.; Stibor, I. Effectiveness of Diverse Mesoporous Silica Nanoparticles as potent Vehicles for the Drug L-DOPA. *Materials* **2019**, *12*, No. 3202.
(48) Vazquez, N. I.; Gonzalez, Z.; Ferrari, B.; Castro, Y. Synthesis of mesoporous silica nanoparticles by sol-gel as nanocontainer for future drug delivery applications. *Bol. Soc. Esp. Ceram. Vidrio* **2017**, *56*, 139−145.
(49) Attard, G. S.; Glyde, J. C.; Goltner, C. G. Liquid-crystalline phase as templates. *Nature* **1995**, *378*, 603−605.
(50) Kao, K. C.; Mou, C. Y. Pore-expanded mesoporous silica nanoparticles with alkanes/ethanol as pore expanding agent. *Microporous Mesoporous Mater.* **2013**, *169*, 7−15.
(51) Thomas, M.; Smarsly, B.; Groenewolt, M.; Ravikovitch, P. I.; Neimark, A. V. Adsorption Hysteresis of Nitrogen and Argon in Pore Networks. *Langmuir* **2006**, 756−764.
(52) Zhang, H.; Li, X. Novel Mesoporous Silica Materials with Hierarchically Ordered Nanochannel: Synthesis with the Assistance of Straight-Chain Alkanes and Application. *J. Chem.* **2016**, *2016*, No. 5146573.
(53) Thommes, M.; Kaneko, K.; Neimark, A. V.; Olivier, J. P.; Rodriguez-Reinoso, F.; Rouquerol, J.; Sing, K. S. W. Physisorption of gases, with special reference to the evaluation of surface area and pore size distribution (IUPAC Technical Report). *Pure Appl. Chem.* **2015**, *87*, 1051−1069.
(54) Ha, C. S.; Park, S. S. *Periodic Mesoporous Organosilicas Preparation, Properties and Applications: General Synthesis and Physico-*

https://doi.org/10.1021/acsomega.1c06492
ACS Omega 2022, 7, 13494−13506

Chemical Properties of Mesoporous Materials; Springer Nature Singapore Pte Ltd.: Singapore, 2019; Vol. *281*.
(55) Cicconi, M. R.; Pili, E.; Grousset, L.; Florian, P.; Bouillard, J. C.; Vantelon, D.; Neuville, D. R. Iodine solubility and speciation in glasses. *Sci. Rep.* **2019**, *9*, No. 7758.
(56) Vaccaro, G.; Agnello, S.; Buscarino, G.; Gelardi, F. M. Thermally induced structural modification of silica nanoparticles investigated by raman and infrared absorption spectroscopies. *J. Phys. Chem. C* **2010**, *114*, 13991−13997.
(57) Guo, C.; Jordan, J. S.; Yarger, J. L.; Holland, G. P. Highly Efficient Fumed Silica Nanoparticles for Peptide Bond Formation: Converting Alanine to Alanine Anhydride. *ACS Appl. Mater. Interfaces* **2017**, *9*, 17653−17661.
(58) Mushtaq, S.; Jeon, J.; Shaheen, A.; Jang, B. S.; Park, S. H. Critical analysis of radioiodination techniques for micro and macro organic molecules. *J. Radioanal. Nucl. Chem.* **2016**, *309*, 859−889.
(59) Dubost, E.; McErlain, H.; Babin, V.; Sutherland, A.; Cailly, T. Recent Advances in Synthetic Methods for Radioiodination. *J. Org. Chem.* **2020**, *85*, 8300−8310.
(60) McIntee, J. W.; Sundararajan, C.; Donovan, A. C.; Kovacs, M. S.; Capretta, A.; Valliant, J. F. A convenient method for the preparation of fluorous tin derivatives for the fluorous labeling strategy. *J. Org. Chem.* **2008**, *73*, 8236−8243.
(61) Jeon, J.; Shim, H. E.; Mushtaq, S.; Choi, M.; Park, S.; Choi, D. J. B.; Jang, B. S. An optimized protocol for the efficient radiolabeling of gold nanoparticles by using a125i-labeled azide prosthetic group. *J. Vis. Exp.* **2016**, *2016*, No. e54759.
(62) IAEA. *Quality Control in the Production of Radiopharmaceuticals*; IAEA: Vienna, Austria, 2018. www.iaea.org/books.
(63) USP. USP Radiopharmaceuticals-proposed-gc-825. In *Radiopharmaceuticals*; USP, 2018; pp 1−62.
(64) Mirshojaei, S. F.; Ahmadi, A.; Morales-Avila, E.; Ortiz-Reynoso, M.; Reyes-Perez, H. Radiolabelled nanoparticles: Novel classification of radiopharmaceuticals for molecular imaging of cancer. *J. Drug Targeting* **2016**, *24*, 91−101.
(65) Mateo, D.; Morales, P.; Ávalos, A.; Haza, A. Comparative cytotoxicity evaluation of different size gold nanoparticles in human dermal fibroblasts. *J. Exp. Nanosci.* **2015**, *10*, 1401−1417.
(66) Dechsakulthorn, F.; Hayes, A.; Bakand, S.; Joeng, L.; Winder, C. In vitro cytotoxicity assessment of selected nanoparticles using human skin fibroblasts. *AATEX J.* **2008**, 397−400.
(67) Piccolo, M.; Misso, G.; Ferraro, M. G.; Riccardi, C.; Capuozzo, A.; Zarone, M. R.; Maione, F.; Trifuoggi, M.; Stiuso, P.; D'Errico, G.; et al. Exploring cellular uptake, accumulation and mechanism of action of a cationic Ru-based nanosystem in human preclinical models of breast cancer. *Sci. Rep.* **2019**, *9*, No. 7006.
(68) Mohammadi, E.; Amanlou, M.; Ebrahimi, S.; Esmaeil, S.; Hamedani, M. P.; Mahrooz, A.; Mehravi, B.; Emami, B. A.; Aghasadeghi, M. R.; et al. Cellular uptake, imaging and pathotoxicological studies of a novel Gd[iii]-DO3A-butrol nano-formulation. *RSC Adv.* **2014**, *4*, 45984−45994.
(69) Choy, J. H.; Kwak, S. Y.; Park, J. S.; Jeong, Y. J. Cellular uptake behavior of [γ-32P] labeled ATP-LDH nanohybrids. *J. Mater. Chem.* **2001**, *11*, 1671−1674.
(70) Aries, A.; Sarmini, E.; Nurmanjaya, A.; Subechi, M.; Sholikhah, U. N.; Lestari, E.; Setiawan, H.; Febriana, S.; Sriyono, S.; Abidin, A. Iodogen Method on Iodine-131 (131I) Radiolabelling of Silver Nanoparticle (AgNPs) as a New Agent of Molecular Imaging. *IOP Conf. Ser.: Mater. Sci. Eng.* **2020**, *924*, No. 012026.
(71) Walsh, A. A. Chemisorption of iodine-125 to gold nanoparticles allows for real-time quantitation and potential use in nanomedicine. *J Nanopart. Res.* **2017**, *19*, No. 152.
(72) Zhang, Y.; Zhang, Y.; Yin, L.; Xia, X.; Hu, F.; Liu, Q.; Qin, C.; Lan, X. Synthesis and bioevaluation of Iodine-131 directly labeled cyclic RGD-PEGylated gold nanorods for tumor-targeted imaging. *Contrast Media Mol. Imaging* **2017**, *2017*, No. 6081724.
(73) Chrastina, A.; Schnitzer, J. E. Iodine-125 radiolabeling of silver nanoparticles for in vivo SPECT imaging. *Int. J. Nanomed.* **2010**, *5*, 653−659.
(74) Xie, L.; Hanyu, M.; Fujinaga, M.; Zhang, Y.; Hu, K.; Minegishi, K.; Jiang, C.; Kurosawa, F.; Morokoshi, Y.; Li, H. K.; et al. 131I-IITM and 211AT-AITM: Two novel small-molecule radiopharmaceuticals targeting oncoprotein metabotropic glutamate receptor 1. *J. Nucl. Med.* **2020**, *61*, 242−248.

https://doi.org/10.1021/acsomega.1c06492
ACS Omega 2022, 7, 13494−13506